NREL
NATIONAL RENEWABLE ENERGY LABORATORY

Relative Lifetime Prediction for CPV Die-Attach Layers

Preprint

Timothy J. Silverman, Nick Bosco,
and Sarah Kurtz

To be presented at the 2012 IEEE International Reliability Physics Symposium
Anaheim, California
April 15–17, 2012

NREL is a national laboratory of the U.S. Department of Energy, Office of Energy Efficiency & Renewable Energy, operated by the Alliance for Sustainable Energy, LLC.

Conference Paper
NREL/CP-5200-54332
March 2012

Contract No. DE-AC36-08GO28308

NOTICE

The submitted manuscript has been offered by an employee of the Alliance for Sustainable Energy, LLC (Alliance), a contractor of the US Government under Contract No. DE-AC36-08GO28308. Accordingly, the US Government and Alliance retain a nonexclusive royalty-free license to publish or reproduce the published form of this contribution, or allow others to do so, for US Government purposes.

This report was prepared as an account of work sponsored by an agency of the United States government. Neither the United States government nor any agency thereof, nor any of their employees, makes any warranty, express or implied, or assumes any legal liability or responsibility for the accuracy, completeness, or usefulness of any information, apparatus, product, or process disclosed, or represents that its use would not infringe privately owned rights. Reference herein to any specific commercial product, process, or service by trade name, trademark, manufacturer, or otherwise does not necessarily constitute or imply its endorsement, recommendation, or favoring by the United States government or any agency thereof. The views and opinions of authors expressed herein do not necessarily state or reflect those of the United States government or any agency thereof.

Available electronically at http://www.osti.gov/bridge

Available for a processing fee to U.S. Department of Energy
and its contractors, in paper, from:

U.S. Department of Energy
Office of Scientific and Technical Information

P.O. Box 62
Oak Ridge, TN 37831-0062
phone: 865.576.8401
fax: 865.576.5728
email: mailto:reports@adonis.osti.gov

Available for sale to the public, in paper, from:

U.S. Department of Commerce
National Technical Information Service
5285 Port Royal Road
Springfield, VA 22161
phone: 800.553.6847
fax: 703.605.6900
email: orders@ntis.fedworld.gov
online ordering: http://www.ntis.gov/help/ordermethods.aspx

Cover Photos: (left to right) PIX 16416, PIX 17423, PIX 16560, PIX 17613, PIX 17436, PIX 17721

Printed on paper containing at least 50% wastepaper, including 10% post consumer waste.

Relative lifetime prediction for CPV die-attach layers

Timothy J Silverman, Nick Bosco and Sarah Kurtz
National Renewable Energy Laboratory
Golden, Colorado 80401

***Abstract*—In concentrating photovoltaics (CPV) cell assemblies, a large-area die-attach layer is subjected to thermal cycles, leading to thermomechanical fatigue. This causes cracking and the eventual failure of the CPV cell by thermal runaway. We define a damage metric representing lumped progress toward failure and present a numerical model for computing the accumulation of damage for arbitrary transient temperature conditions. The model is applied to a particular design with a solder die-attach layer. We show that accelerated-test thermal cycles with higher ramp rates cause more damage, both per cycle and per unit time. Outdoor exposure to one entire year in two geographic locations is also simulated, revealing that a year of exposure in Golden, Colorado is equivalent to 1.4 years of exposure in Oak Ridge, Tennessee.**

I. Background and introduction

In concentrating photovoltaic (CPV) systems, small solar cells are exposed to sunlight that has been optically concentrated. Typical high-concentration CPV systems use approximately 1 cm^2 cells under sunlight concentrated by 500× to 1000×. In a typical cell, 40% of the light incident on the cell is converted to electricity and the remaining 60% is dissipated as heat. Effective removal of this heat is critical for the cell to continue functioning. The components of the cell assembly, namely the cell, die-attach material and substrate, all have different coefficients of thermal expansion. Cyclic changes in the temperature of the assembly result in differential thermal expansion, subjecting the assembly to thermomechanical fatigue. Cracking of the die-attach material due to thermomechanical fatigue has been suggested as a key failure mechanism for some CPV systems [1], [2].

CPV products sold today have not existed long enough for adequate reliability prediction based on field data. Instead, designs are evaluated using indoor accelerated tests, such as thermal cycling, that have been developed to duplicate failures observed in the field for early designs. The accelerated test protocols used in qualification testing are intended to expose faulty design, materials and workmanship, not to predict lifetime [3]. A quantitative connection between the die-attach material's lifetime during accelerated testing and during outdoor exposure has not been made. Furthermore, CPV systems can be deployed in widely varying meteorological conditions. The sensitivity of a cell assembly's lifetime to its service conditions has also not been established.

In this paper, we present results from a computational model of thermomechanical fatigue in a CPV cell assembly. The model describes the viscoplastic behavior of a solder die-attach layer and quantifies the damage sustained by the layer during arbitrary temperature conditions. To provide information on how to most quickly complete accelerated tests, we make quantitative comparisons of die-attach layer lifetime by computing the accumulated damage for temperature histories typical of accelerated testing and of outdoor exposure in various climates. For accelerated test cycles, we examine the sensitivity of the rate of damage accumulation to the ramp rate and dwell time of the thermal cycle.

II. Method

A. Failure mechanism and metric

The failure mechanism under consideration is cracking in the die-attach layer. In CPV applications, solder or conductive epoxy can serve as the die-attach material. Compared to the relatively well-understood solder joints used in microelectronics packaging, CPV die-attach layers are large and cracks cause device failure in a different way. A microelectronics package has failed when a single, critical solder joint, often the outermost in a pattern of hundreds of <1 mm solder balls, develops a through crack [4], [5]. In contrast, CPV cells are often ∼1 cm square and their entire areas are attached to a substrate with a large-area die-attach layer. The CPV cell assembly has failed when, in a corner of the die-attach layer, a crack develops that is large enough to cause the failure of the solar cell due to thermal runaway.

The size of the crack needed to cause thermal runaway thus depends on the characteristics of the cell, the assembly and service conditions such as electric current density. In one particular cell assembly, it has been shown that a void or crack covering 2.5%–4% of the die-attach area, depending on the die-attach material, is sufficient to cause thermal runaway during operation [6]. The objective of this work is to predict, given a particular cell assembly design, the relative time to failure of the package when exposed to different service conditions.

The choice of solder composition influences the fatigue life of the die-attach layer. Compared to a lead-based solder joint, the lifetime of a lead-free solder connection can be several times shorter or longer depending on service or test conditions [7]. Eutectic and near-eutectic lead-tin solders are a common choice of die-attach material and we select the 60Sn40Pb composition for this investigation. Lead-tin solder shows substantial viscoplastic behavior at CPV service temperatures.

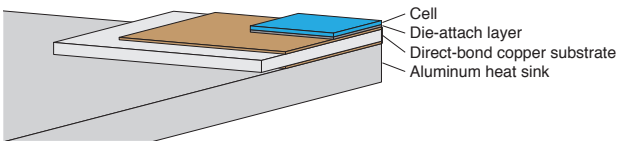

Fig. 1. Simplified representation of the CPV cell assembly model used in this work. One quarter of the assembly is shown and optical elements and electrical connections are hidden.

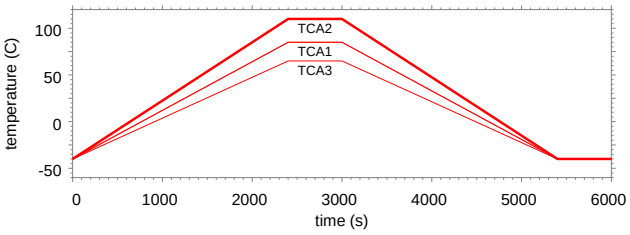

Fig. 2. Accelerated-test thermal cycles prescribed by IEC 62108.

This results in time-independent, time-dependent and rate-dependent inelastic deformations. Producing these deformations requires the dissipation of inelastic work, which has been proposed as a measure of damage in solder connections [5]. In each of the three normal and three shear directions, inelastic strain energy density, also called inelastic work, is defined as

$$W_{\text{pl}} = \int |\sigma| \, d\varepsilon_{\text{pl}} \ , \tag{1}$$

where σ is normal or shear stress and ε_{pl} is the inelastic component of normal or shear strain. Work done in the in-plane directions acts primarily in the interior of the die-attach layer or parallel to cracks, so it does not contribute to crack growth in the area of interest. Thus the appropriate measure of damage is the volume average of the sum of the three out-of-plane inelastic energy density components, which has units of J m^{-3} or Pa. This damage metric excludes most of the inelastic work done in the interior of the solder layer, eliminating the need to arbitrarily establish a geometric region in which to measure damage.

In this investigation we use the damage quantity to reflect lumped progress toward failure and we ignore the details of crack initiation and propagation. We propose that a typical cell assembly will fail after it has sustained a characteristic quantity of damage. By comparing the damage done by exposure to various thermal conditions, a given assembly's relative lifetime in those conditions can be estimated.

B. Simulation

We calculate the accumulation of damage in the die-attach layer by simulating the solid mechanics of the layer using the finite element method. The three-dimensional geometry is shown schematically in Fig. 1. We neglect electrical connections, encapsulant and optical elements at the top of the cell and assume a flawless solder layer, free of voids, contamination and pre-existing cracks.

We use the Anand model to compute the viscoplastic material response in the solder layer. The solder layer contains a field of inelastic strain that is superposed with the elastic strain field. The rate of change of equivalent inelastic strain follows the flow equation,

$$\dot{\varepsilon}_{\text{pl,eq}} = A \exp\left(\frac{-Q}{RT}\right) \left[\sinh\left(\xi \frac{\sigma_{\text{eq}}}{s}\right)\right]^{\frac{1}{m}} \ , \tag{2}$$

where A is a pre-exponential factor, Q is an activation energy, R is the ideal gas constant, T is temperature, ξ is a stress factor, σ_{eq} is equivalent stress, s is a hardening variable and m is a sensitivity exponent. This equivalent inelastic strain rate is partitioned into the six inelastic strain rate components using

$$\left(\dot{\varepsilon}_{\text{pl}}\right)_{ij} = \frac{3}{2} \dot{\varepsilon}_{\text{pl,eq}} \frac{(\sigma_d)_{ij}}{\sigma_{\text{eq}}} \ , \tag{3}$$

where $\left(\dot{\varepsilon}_{\text{pl}}\right)_{ij}$ is the rate of change of the ij component of inelastic strain and $(\sigma_d)_{ij}$ is the ij component of σ_d, the deviatoric stress [8].

The hardening variable s is a field in the solder layer representing isotropic resistance to deformation. It has units of stress and evolves according to

$$\begin{aligned} \dot{s} &= \dot{\varepsilon}_{\text{pl,eq}} \ h_0 \left|1 - \frac{s}{s^*}\right|^a \ \text{signum}\left(1 - \frac{s}{s^*}\right) \\ s^* &= \hat{s} \left[\frac{\dot{\varepsilon}_{\text{pl,eq}}}{A} \exp\left(\frac{Q}{RT}\right)\right]^n \ , \end{aligned} \tag{4}$$

where h_0 is a hardening constant, a is a factor for the sensitivity of hardening to strain rate, s^* is the variable saturation value of hardening, $\hat{s}$ is a hardening saturation coefficient and n is a sensitivity exponent.

We use values for the material properties, A, Q, ξ, m, h_0, a, $\hat{s}$, n, fitted to experiments on 60Sn40Pb solder [9]. These properties are assumed to remain stationary throughout the life of the device. The germanium cell and direct-bond copper (DBC) substrate layers are assumed to behave elastically. The assembly has two planes of symmetry, so only a quarter of the geometry is simulated. The effect of the heat sink on the mechanical response of the cell assembly is neglected; mechanically, the assembly is simply supported.

The aluminum heat sink, shown in Figure 1, is the component of the CPV cell assembly that faces the ambient air. We refer to the outside temperature of the heat sink as the *module temperature* and the temperature of the CPV cell as the *cell temperature*.

Accelerated testing of CPV modules is done according to the IEC 62108 standard, which prescribes the thermal cycles shown in Figure 2. The TCA1, TCA2 and TCA3 cycle types have a maximum temperature of 85, 110 and 65°C, respectively. All of the cycles use a minimum temperature of −40°C and a dwell time of 10 minutes. The standard allows for a range of total cycle times; we select 100 minutes as a baseline cycle time. These tests are performed without illumination; the specimen is heated and cooled by the surrounding air. The standard calls for the application of current during certain portions of the thermal cycle; we ignore the local temperature

variations that this would cause. Considering the small mass and thickness of the cell assembly and the modest ramp rates of the accelerated test cycles, we assume the cell and module temperatures are equal and that the cell assembly's temperature is uniform during accelerated test cycles. We simulate the damage accumulated in the die-attach layer during the three standard types of accelerated test cycles and consider changes to the timing of the standard cycles. We show that the damage done by a single thermal cycle depends on the model's state, namely the field of $\left(\varepsilon_{\mathrm{pl}}\right)_{ij}$ and s in the solder layer. The physical initial state cannot be perfectly determined ahead of time, so an approximate initial state must be chosen. The damage done per repetition of a thermal cycle then settles to a constant value over the course of several cycles. In every analysis of a thermal cycle presented here, we simulate at least 25 cycles and present the damage done by the final cycle. In this work, figures for damage and for damage rate, defined here as $\frac{\text{damage per cycle}}{\text{cycle time}}$, are always normalized to the damage or damage rate for a single TCA2 cycle as shown in Figure 2.

For simulation of outdoor exposure, the module temperature is calculated from one-minute measurements of ambient temperature, wind speed and direct normal irradiance (DNI) using a model based on a steady-state model for CPV systems [10]. To capture transient behavior, an exponential weighted moving-average (EWMA) filter with a time constant derived from experimental CPV module temperature data is applied to the static model. Because the cell's temperature responds to changes in DNI almost instantaneously, the cell temperature is computed from the module temperature by adding a static contribution proportional to DNI and fitted from experiment. Module temperature (T_m) and cell temperature (T_c) at time step t are calculated using

$$\begin{aligned}\left(T_m\right)_t &= \alpha\left\{\left(T_a\right)_t + \left(E_{\mathrm{DNI}}\right)_t \exp\left[a + b\left(v_w\right)_t\right]\right\} + \left(1-\alpha\right)\left(T_m\right)_{t-1} \\ \left(T_c\right)_t &= \left(T_m\right)_t + \Delta T_c \frac{\left(E_{\mathrm{DNI}}\right)_t}{\left(E_{\mathrm{DNI}}\right)_{\mathrm{ref}}} \ ,\end{aligned} \tag{5}$$

where α is the EWMA gain, T_a is ambient temperature, E_{DNI} is direct normal irradiance, v_w is wind speed, a and b are fitting coefficients and ΔT_c is the cell temperature rise at the reference irradiance, $\left(E_{\mathrm{DNI}}\right)_{\mathrm{ref}}$.

The difference between T_m and T_c introduces a gradient in temperature between the top and bottom layers of the cell assembly. Preliminary simulations showed that neglecting this gradient can cause damage to be underestimated by more than 35% in certain weather conditions. We assume the through-plane temperature distribution at any moment matches the one-dimensional, steady-state heat conduction solution for the cell assembly layers without thermal contact resistance. Preliminary simulations of the three-dimensional, transient heat conduction problem showed the validity of this approximation due to the cell assembly's small mass and large aspect ratio.

We synthesize a year of module and cell temperature data using weather data from July 2008 through June 2009. The year is made periodic by adjusting the conditions at the beginning and end of the year until they match. The periodic year is simulated until the results from the final day match those from the same day in the previous year. This typically takes $\sim$1.2 simulated years.

III. Results and discussion

A. Accelerated test cycles

Accelerated testing can be made more economical by choosing cycles that cause more damage. The *rate* of damage accumulation, not the absolute damage done by each cycle, is the parameter to be maximized.

1) Dwell time effect: We simulated accelerated test cycles based upon the IEC 62108 type TCA1, TCA2 and TCA3 cycles, but with changes to the hot and cold dwell times. The modified temperature cycles and resulting accumulation of damage are shown in Figures 3 and 4. In Figure 3, cycles with a hot dwell time of 600 s and cold dwell times of 0, 600 and 6000 s are shown. In Figure 4, cycles with a cold dwell time of 600 s and hot dwell times of 0, 600 and 6000 s are shown. In every case, a longer dwell time enables a test cycle to do more damage. The effect of extending the cold dwell time is stronger for higher-temperature cycles (TCA2) whereas the effect of extending the hot dwell time is stronger for lower-temperature cycles (TCA3).

The rate of accumulation of damage for each variation of dwell time is shown in Figure 6, normalized to the damage rate for the TCA2 cycle. Changing the hot dwell time has a minimal effect on damage rate. For a TCA2-type cycle, changing the cold dwell time to 0 s increases the damage rate by 9%.

Stress in the solder layer relaxes during the hot dwell period, enabling high stresses to develop during the cooling ramp, during which the majority of the damage in the standard cycle is done. But the high temperature of accelerated test cycles enables substantial stress relaxation to occur even when the hot dwell time is zero. Thus the damage per cycle is relatively insensitive to changes in the hot dwell time.

The kinetics of plastic flow in the solder are slowed at low temperatures, so stress relaxation occurs more slowly during the cold dwell period. Increasing the cold dwell time allows more relaxation to occur, enabling the heating ramp to accumulate more damage. However, this requires a much longer cycle time, meaning that only modest increases in the damage rate can be achieved by extending the cold dwell time. In summary, Figure 6 shows that the damage rate is not particularly sensitive to changes in dwell time. These results apply to the specific material system and geometry simulated here. It has been shown that the optimal dwell time depends on solder composition [11].

2) Ramp rate effect: The accelerated test cycles were modified by altering the ramp rates between the hot and cold dwell periods. The modified cycles and the resulting accumulation of damage are shown in Figure 5. The standard cycle's ramp time is 40 minutes. Cycles with 20-, 10- and 5-minute ramp times are also shown in Figure 5. Increasing the ramp rate increases the damage done per cycle by increasing the damage

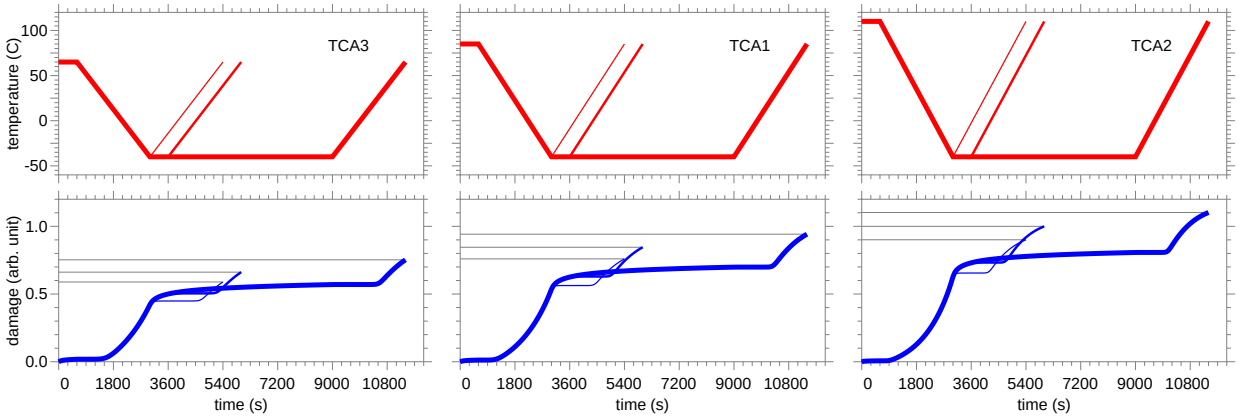

Fig. 3. Accelerated-test thermal cycles modified with different cold dwell times of 0, 10 and 100 minutes. Damage is normalized to the baseline TCA2 cycle, a cycle with a 10-minute cold dwell time. Extending the cold dwell increases the damage done by a given cycle by allowing more stress relaxation to occur.

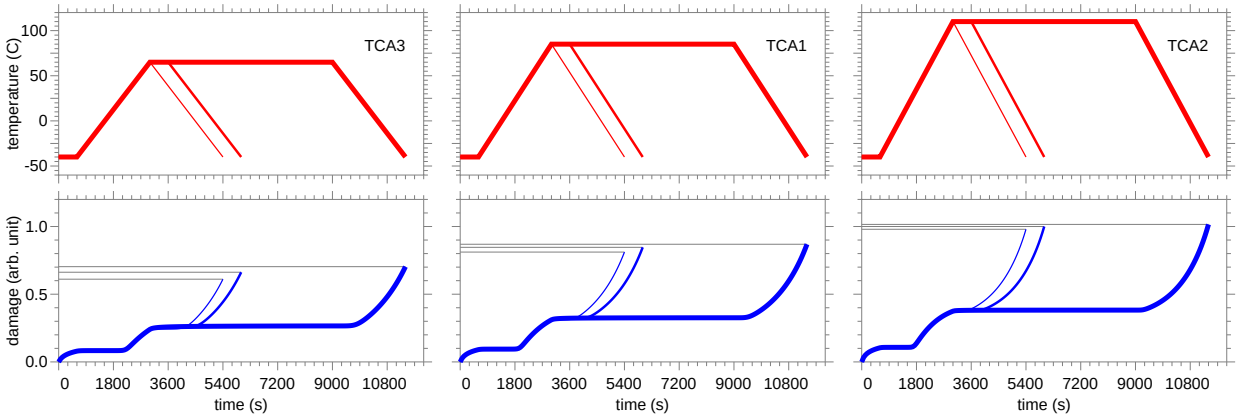

Fig. 4. Accelerated-test thermal cycles modified hot dwell times of 0, 10 and 100 minutes. Damage is normalized to the baseline TCA2 cycle, a cycle with a 10-minute hot dwell time. Extending the hot dwell increases the damage done by a given cycle by allowing more stress relaxation to occur. The effect is stronger for the low-temperature cycle (TCA3) than for the high-temperature cycle (TCA2).

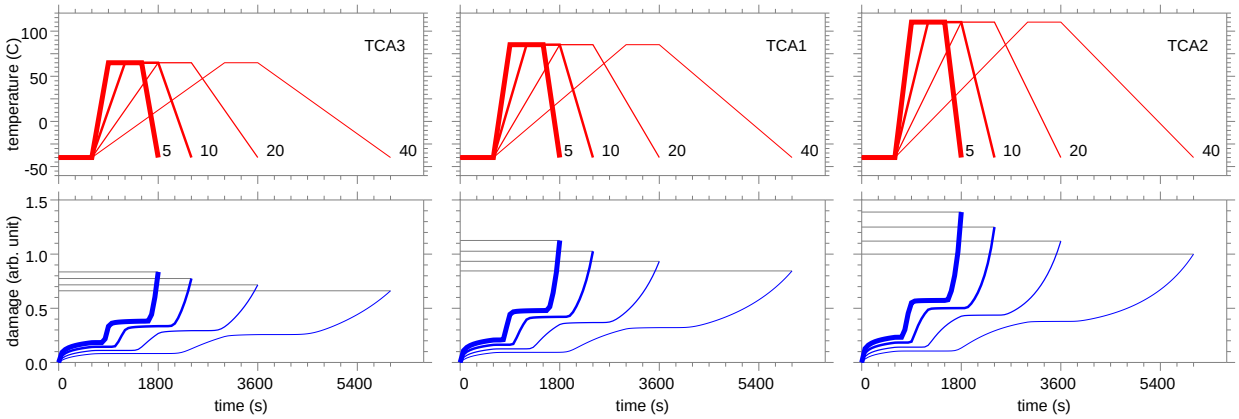

Fig. 5. Accelerated-test thermal cycles modified with different ramp times. Temperature curves are marked with the ramp time in minutes. Damage is normalized to the baseline cycle, a TCA2 cycle with a 40-minute ramp time. Shorter ramps result in substantially more damage per cycle.

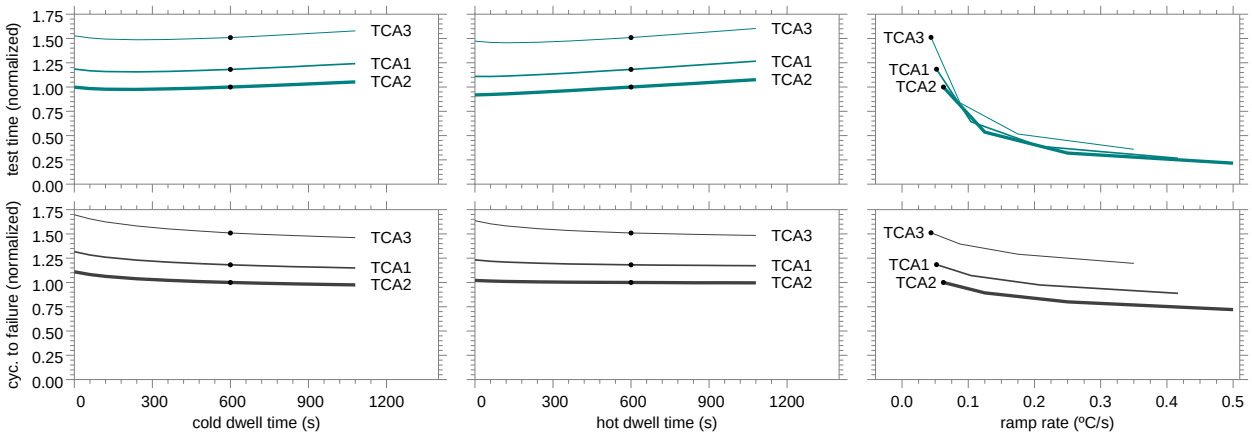

Fig. 6. Test time and cycles to failure, normalized to the baseline TCA2 cycle, for modified accelerated test cycles with variable ramp rates and dwell times. The baseline cycle for each cycle type is marked with a point. Increasing a cycle's ramp rate can substantially reduce test time.

done during both ramps. The effect is stronger with higher-temperature cycles.

The rate of accumulation of damage for the cycles with modified ramp rates is shown in Figure 6. Changing the ramp time of a TCA2 cycle to 5 minutes, a ramp rate of 0.5°C/s, increases the damage rate of the cycle by more than 450% compared to the same cycle with a 40-minute ramp time.

For every cycle tested here, the damage rate increases with increasing ramp rate. Faster changes in temperature cause higher stresses to develop in the solder layer before plastic flow can cause them to relax, causing more damage during the ramp period. More damage is also done during the dwell periods because the solder layer is subjected to higher stress at the beginning of each dwell period. However, achieving test cycle ramp rates as high as 0.5°C/s may be technically difficult, particularly with test equipment that is designed for the standard cycles. Unconventional test equipment, such as equipment that tests only the cell assembly instead of the entire module or equipment that heats the cells with forward bias, can achieve even higher ramp rates, but at the cost of temperature uniformity through the assembly and possible excitation of a thermal shock failure mechanism. In summary, Figure 6 shows that the highest damage rate is achieved with the highest practical ramp rate that does not excite a different failure mechanism from the service failure mechanism. The simulation tools presented here may be used to identify the onset of uncharacteristic failure mechanisms: when test articles fail much sooner than the simulations predict, a different, unmodeled mechanism may be responsible.

In typical empirical models, the effect of dwell time and ramp rate is lumped into a single cycling frequency term with a strictly negative relationship to the accumulation of damage [12]. The preceding results indicate a large difference in their respective sensitivities and that the cumulative effect may in fact be of opposite sign. Therefore both dwell time and ramp rate should be considered independently when the effect of the cycling frequency on the rate of damage accumulation (acceleration factor) is analyzed.

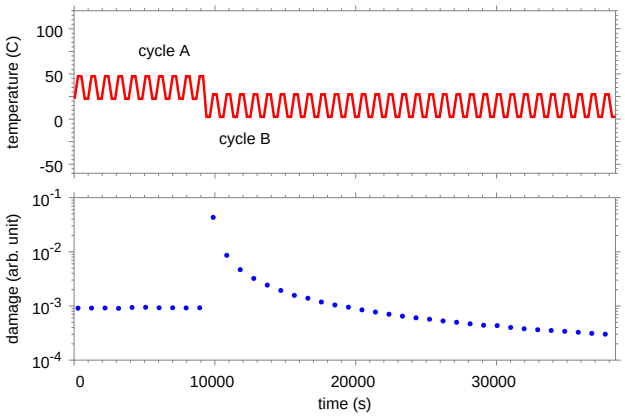

Fig. 7. Switching from one thermal cycle to another affects the damage done by each cycle in a transient way.

3) Cycle switching: We simulated many repetitions of a small thermal cycle (cycle A), followed by many repetitions of a similar thermal cycle with a different mean temperature (cycle B). The temperature history and damage per cycle are plotted in Figure 7. The damage done by the first instance of cycle B is more than two orders of magnitude greater than the long-term characteristic damage of cycle B.

The damage done by a particular cycle depends not only on the nature of the cell assembly and the cycle, but also on the solder layer's internal state. The internal state includes the six components of inelastic strain and the hardening variable s at every location. For a given material and geometry, each thermal cycle results in a cycle of s with a particular mean value. The s cycle does not reach its long-term amplitude and mean until after many repetitions of the thermal cycle. Since the damage done by a given cycle depends on the present field of s in the solder layer, the amount of damage done by the cycle is only constant after the s cycle has reached its long-term amplitude and mean.

The damage done by a long sequence of thermal cycles can

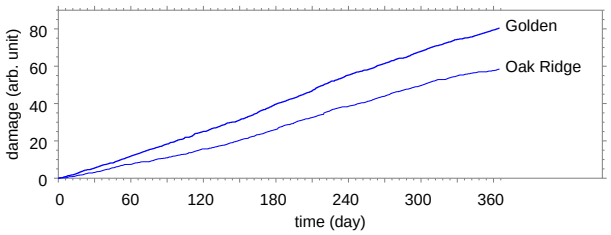

Fig. 8. Accumulated damage for one year of outdoor exposure in two different locations. The weather data are taken from June 2008 through July 2009.

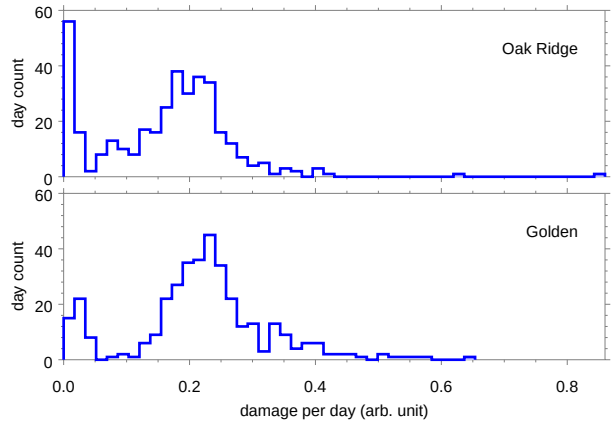

Fig. 9. Histograms of the daily accumulated damage.

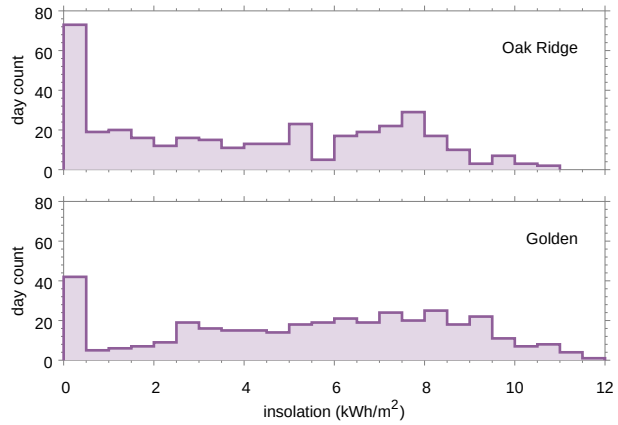

Fig. 10. Histograms of the direct component of insolation.

thus be approximated by multiplying the damage done by a single such cycle after the specimen has reached its long-term state *s*. Efforts have been made to compute the damage done during outdoor exposure by assigning to each temperature reversal an amount of damage corresponding to the damage done by a long sequence of such reversals. We have now shown that this will result in a miscalculation of damage because the temperature reversals during outdoor exposure never repeat in a long sequence and can occur in any order.

B. Outdoor exposure

One entire year of outdoor exposure was simulated for Golden, Colorado and for Oak Ridge, Tennessee in the United States. The accumulated damage is shown in Figure 8. For the mechanism considered here, a year of outdoor exposure in Oak Ridge is equivalent to ∼59 TCA2 thermal cycles. A year in Golden is equivalent to ∼80 TCA2 thermal cycles or 1.4 years in Oak Ridge. No uncertainty analysis has been done regarding these predictions, so confidence in the relative lifetime between locations is higher than confidence in the absolute number of equivalent thermal cycles.

Cell temperature histories and damage accumulation for selected days in the two locations are shown in Figures 11 and 12. The uppermost plots show days where practically no damage occurs because the DNI and ambient temperature, and thus the cell temperature, remain low for the entire day. Examples of clear days are shown next. For both locations, the sunny day causes very nearly the median damage for all days of the year. The third row of plots shows partly-cloudy days causing relatively heavy damage due to multiple transitions between very low and very high DNI. The final row shows the most damaging day of the year for each location. These days are characterized by high ambient temperatures and a period of full sun in the morning followed by several hours of sharp transitions between full sun and virtually no sun.

As with accelerated test cycles, most of the damage done during a sunny day occurs during the cooling ramp, after stress relaxation has occurred at elevated temperature. Sunny days with periods of opaque clouds provide multiple heating and cooling phases, each of which causes damage according to its ramp rate and dwell time. The most damaging days have the greatest number of transitions between full sun and virtually no direct sun.

Given that the same qualitative day types are present and do approximately the same amount of damage in both locations, the difference in total annual damage accumulation between the two cities is due to differing numbers of days of each type. Histograms of the daily amount of accumulated damage are shown in Figure 9. Compared to Golden, Oak Ridge has a greater number of days during which very little damage is done. Golden has a higher median daily damage than Oak Ridge.

We quantify the total amount of energy available to heat the cell above ambient temperature by integrating DNI to obtain the direct component of insolation. The histogram of insolation for the year simulated here is shown in Figure 10. Over the course of the year, Golden has 36% more direct insolation than Oak Ridge. In summary, a year in Golden does more damage than a year in Oak Ridge in part because Golden has more sunny days and more days of highly variable irradiance.

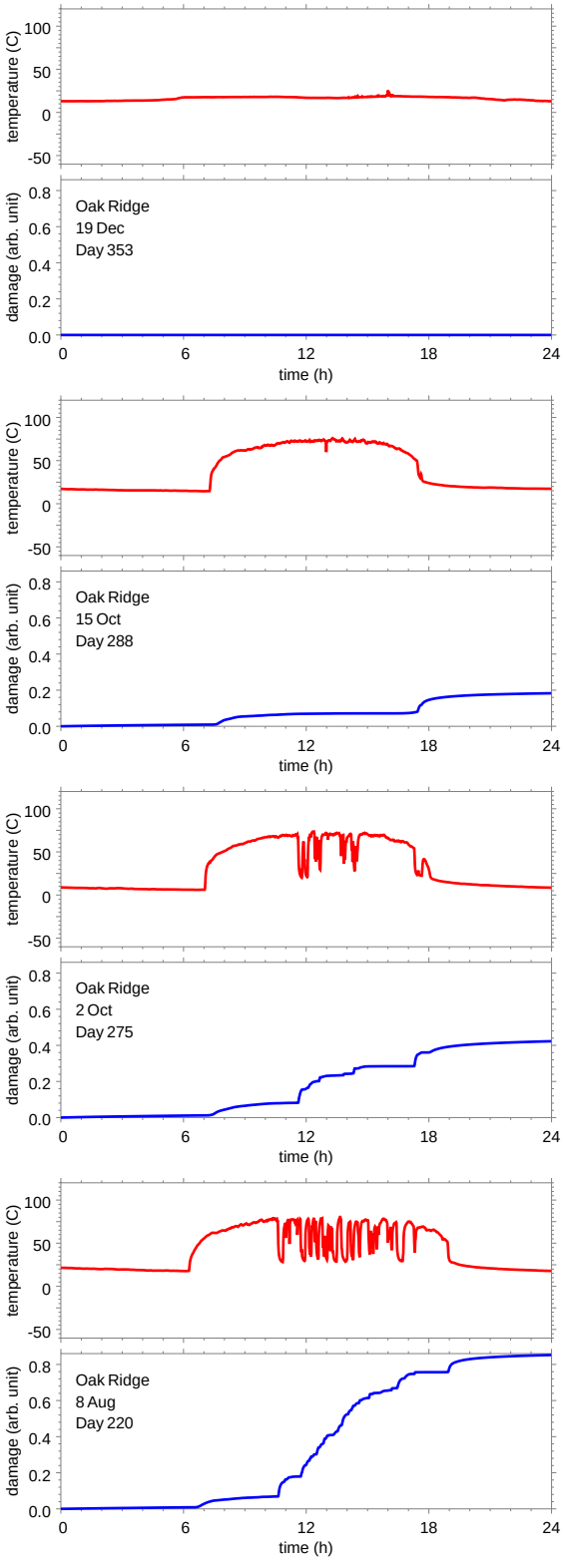

Fig. 11. Temperature histories and damage accumulation for selected days in Oak Ridge.

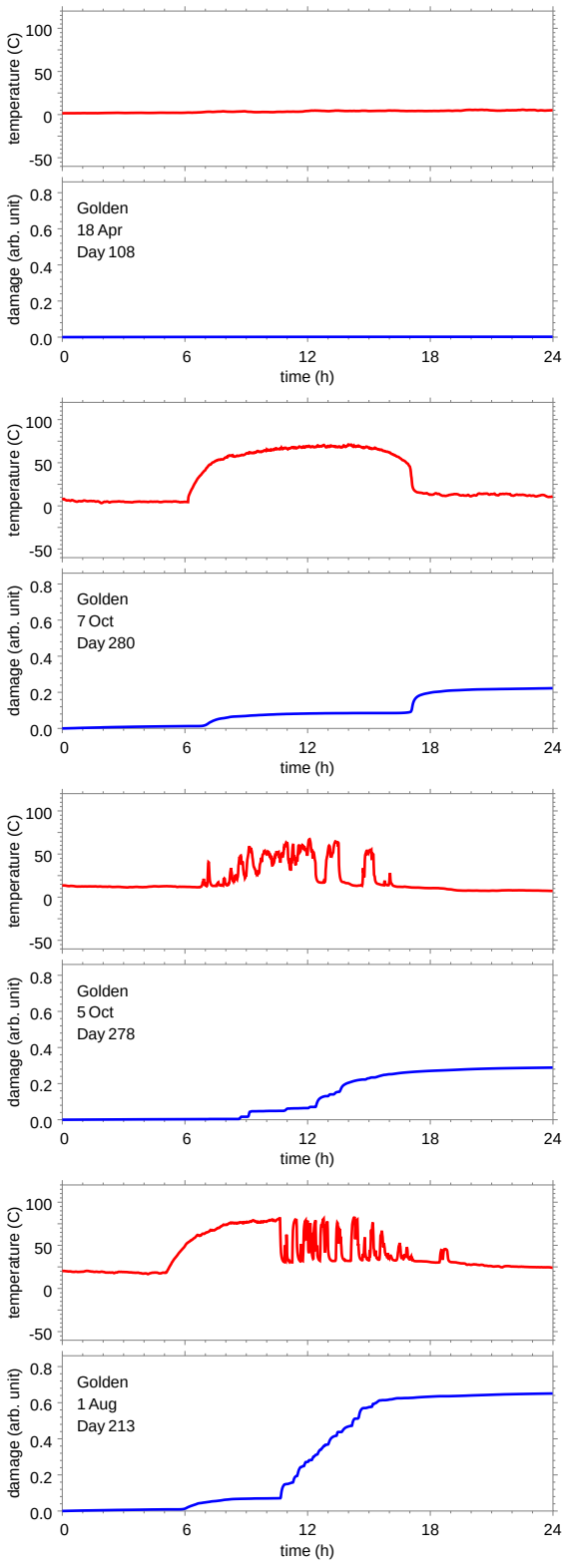

Fig. 12. Temperature histories and damage accumulation for selected days in Golden.

IV. Conclusion

We have shown how different kinds of temperature changes cause different amounts of damage in the CPV die-attach layer. Thermal cycles with long dwell times and fast ramp rates cause more damage per cycle than those with short dwell times and slow ramp rates. When damage per cycle is divided by total cycle time, the resulting damage rate is weakly dependent on dwell time, but still strongly correlated with ramp rate.

During outdoor exposure, sunny days punctuated with opaque clouds cause much more damage per day than clear days, which in turn cause more damage than very cloudy days. The number of days of each type in a particular location determines the total annual accumulation of damage in that location. One year of outdoor exposure in Golden, Colorado causes as much damage as approximately 1.4 years in Oak Ridge, Tennessee.

Acknowledgment

The authors acknowledge support from Amonix, the United States Department of Energy and the California Solar Initiative for this work.

References

[1] N. Bosco, T. Silverman, and S. Kurtz, "Modeling thermal fatigue in CPV cell assemblies," in *Photovoltaic Specialists Conference*, 2011.

[2] M. Cao, S. Butler, J. Benoit, Y. Jiang, R. Radhakrishnan, Y. Chen, and S. Bendapudi, "Application of Anand-type viscoplastic solder material model for thermal stress analysis/life prediction of concentrating photovoltaic (CPV) module." ASME, 2007.

[3] IEC 62108, "Concentrator photovoltaic (CPV) modules and assemblies - Design qualification and type approval," IEC Standard, 2007.

[4] D. S. Steinberg, *Preventing thermal cycling and vibration failures in electronic equipment*. New York: John Wiley and Sons, Inc., 2001.

[5] Perkins, *Solder Joint Reliability Prediction for Multiple Environments*. Springer, 2009.

[6] N. Bosco, C. Sweet, T. Silverman, and S. Kurtz, "CPV cell infant mortality study," in *7th International Conference on Concentrating Photovoltaic Systems (CPV-7)*, 2011.

[7] J. Clech, "Lead-free and mixed assembly solder joint reliability trends," *IPC Apex, February*, 2004.

[8] G. E. Totten, L. Xie, and K. Funatani, Eds., *Modeling and simulation for material selection and mechanical design*. New York: Marcel Dekker, Inc., 2004, ch. 4.

[9] G. Wang, Z. Cheng, K. Becker, and J. Wilde, "Applying Anand model to represent the viscoplastic deformation behavior of solder alloys," *Journal of electronic packaging*, vol. 123, p. 247, 2001.

[10] D. King, W. Boyson, and J. Kratochvill, "Photovoltaic array performance model," Sandia Naitonal Laboratories, Tech. Rep. SAND2004-3535, 2004.

[11] J. Clech, "Acceleration factors and thermal cycling test efficiency for lead-free sn-ag-cu assemblies," in *Proceedings, SMTA international conference, Chicago, IL*, 2005, pp. 902–917.

[12] K. Norris and A. Landzberg, "Reliability of controlled collapse interconnections," *IBM Journal of Research and Development*, vol. 13, no. 3, pp. 266–271, 1969.